Small fire ant rafts are unstable

Hungtang Ko, Mathias Hadgu, Keyana Komilian, and David L. Hu

Phys. Rev. Fluids **7**, 090501 — Published 20 September 2022

DOI: 10.1103/PhysRevFluids.7.090501

Small fire ant rafts are unstable

Hungtang Ko[1], Mathias Hadgu[1], Keyana Komilian[2], and David L. Hu[1,3]
[1]Woodruff Schools of Mechanical Engineering, Georgia Institute of Technology
[2]Coulter Department of Biomedical Engineering, Georgia Institute of Technology
[3]School of Biological Science, Georgia Institute of Technology

August 23, 2022

Abstract

In this combined experimental and numerical study, we film the formation of fire ant rafts to determine how they cohere together. Surprisingly, we discover that ants prioritize separation and exploration: they flail legs and bounce off neighbors when they collide. Despite the active repulsion, Fire ants cohere by the Cheerios effect, a capillary force that attracts small floating objects such as breakfast cereal. Experiments reveal that rafts consisting of fewer than ten ants disintegrate within minutes. Predictions by a Langevin model reproduce the stability transition and the critical raft size, which emerges from the balance between their mutual repulsion and the Cheerios effect. This work may inspire physically grounded models for the behavior of natural swarms.

Introduction

Animal groups accomplish tasks that individuals cannot achieve [1, 2, 3]. For example, army ants link their bodies to build bridges over gaps [4]. Slime molds *Dictyostelium discoideum* distribute their spores by building fruiting bodies to grow in height by a factor of 200 [5, 6]. Fish schools reduce energy expenditure and facilitate evasion of predators [7, 8, 9]. One way that we recognize a flock of birds or a school of fish is by its cohesion [10]: members of a swarm remain together despite changes in the swarm's shape and internal structure. Although cohesion in natural swarms is a simple enough concept to recognize, the mechanism by which it arises is still a mystery. Understanding how individuals cohere may inspire new swarm models and guide the designs of artificial systems. The goal of this study is to investigate the origin of cohesion in fire ant rafts.

Currently, most models of swarms require a "social force" that attracts individuals towards their neighbors or the center of the swarm [11, 12, 13, 14, 15, 16]. The 1995 Vicsek model [17] does not feature social attraction and thus swarms behave unrealistically: they disperse in the open space [18, 11, 19]. A social attraction force is fundamentally different from physical forces such as drag and thrust. It involves a cascade of internal signals in which the animal senses the distance to its neighbors and propels itself to maintain that distance. Social attraction forces have long been used to rationalize the motion of fish schools [20, 21, 22, 23], bird flocks [24, 25, 26], and insect swarms [27]. Although social attraction enables models to emulate various collective behaviors, Lopez et al. [28] cautioned that this approach increases the number of model parameters to be measured from experiments. Furthermore, as a proxy for complex animal interactions and sensory feedback, social attraction is in itself an emergent property. It may be difficult to justify social attraction forces for insect swarms, for which individuals have limited sensing capabilities and intelligence. Despite years of work, it remains unknown if social attraction forces are legitimate or simply a crutch. In this work, we rationalize the formation of ant rafts without invoking social attraction.

We perform experiments with red imported fire ants (*Solenopsis invicta*, **Figure 1**A). Native to the Pantanal wetlands in Brazil [29], this invasive species can now be found on all continents except for Antarctica [30]. Fire ants can link their bodies together to build rafts, towers, and bridges. Ants

on the raft perform random walks and expand the raft by accretion of their bodies on the raft edge [31]. Fire ants may also extend pseudopod-like appendages through treadmilling [32] and morph into streamlined airfoil shapes when in flow [33]. Previous studies have focused on large rafts with more than 1000 ants [31, 34, 32] but did not discuss how rafts stayed together. In this study, we focus on rafts with size 2 to 158 ants to better understand the mechanisms of raft formation.

Results

Experimental observations: Small rafts are not stable

We filmed the behavior of balls of ants placed on the water surface (Movie S1). In total, we performed 72 experiments involving groups ranging from 2 to 158 ants. Surprisingly, we find that ant rafts are only stable if they contain at least $N_c \approx 10$ ants. **Figure 1**C shows a time series of a raft of five ants breaking apart when placed on the water surface. The dense ant ball expands rapidly as it contacts the water surface, and then ants begin to disperse in all directions. **Figure 1**B shows the relationship between N, the number of ants initially in a raft, and P, the proportion of ants that leave the raft after five minutes. Experimental data are shown by orange triangles. Clearly, larger rafts are more stable, with a stark transition to stability at ten ants. Phenomenologically, such a trend is shown by a logistic function(**Figure 1**B),

$$P(N) = \frac{1}{1 + e^{(N-N_c)/\Delta N}}, \tag{1}$$

where N_c is the critical number of ants for stability, and ΔN is the width of the transition interval. Note that when $N = N_c$, half of the ants go astray ($P = 0.5$). The dashed orange line shows a least-squares fit to our experiments. The best fit yields $N_c = 9.3$ and $\Delta N = 1.5$ ($n = 72, R^2 = 0.66$).

To better understand the factors that lead to the critical raft size, we film the interaction between pairs of ants as they encounter each other on the water surface. Each pair of ants separates after an average interaction time of 77 ± 69 seconds ($n = 14$). The interaction time is highly variable, ranging from as little as 10 seconds up to four minutes. During this interaction, they flail their legs, intermittently colliding with each other before ultimately departing in opposite directions. This observation contradicts with the naïve assumption that all swarming individuals have social attraction.

To determine the dominant forces on the ants, we calculate common dimensionless groups. The Reynolds number $\mathrm{Re} = Ul/\nu \sim 10$, where $l \sim 3$ mm is an ant's characteristic body length, $U \sim 4$ mm/s its characteristic swimming speed, and ν the kinematic viscosity of water. The Reynolds number suggests that both inertia and viscous force influence an ant's motion. Indeed, when pushed manually, dead ants can drift for tens of body lengths through their inertia. The Reynolds's number remains small if other characteristic length scales are considered such as the body width $w = 1$ mm, or the leg width $w' = 100$ µm. The Bond number $\mathrm{Bo} = \rho g l^2/\gamma \sim 1.3$ where ρ is the density of water, g is the gravitational acceleration, and γ is the surface tension of water. The Bond number suggests that both surface tension and buoyancy contribute to the weight support of the ants. Indeed, we see that fire ants maintain their position mostly above the water surface, with just their legs' tips and ventral surfaces wetted. From here on, we will characterize their motion on the water as walking rather than swimming.

A Langevin model describing fire ant interactions

We proceed by presenting a model for raft formation that does not rely on social attraction. The goal of our model is to rationalize the critical number of ants N_c for raft cohesion as well as the effect of different parameters such as ant activity level and initial spacing. Newton's law applied to a single ant of mass $m \approx 1$ mg states:

$$m\ddot{\boldsymbol{x}}_i = k_a\boldsymbol{\eta}_i - k_f\dot{\boldsymbol{x}}_i - \sum_{i\neq j} k_c \mathrm{K}_1(|\boldsymbol{d}_{ij}|/l_c)\hat{\boldsymbol{d}}_{ij} + \sum_{i\neq j, d_{ij}<2r} k_r \boldsymbol{d}_{ij} \tag{2}$$

$$\text{inertia} = \text{propulsion} + \text{drag} + \text{capillary} + \text{repulsion}$$

where $\boldsymbol{x_i}$ is the two-dimensional position of ant i and $\ddot{\boldsymbol{x}}_i$ is its acceleration. The forces experienced by the ants include propulsion, viscous drag, capillary attraction, and ant-to-ant repulsion. These four terms are characterized by their corresponding coefficients k_a, k_f, k_c, and k_r.

Active propulsion

In Equation (2), the first term on the right-hand side is the random propulsive force of ants. Dropping the i subscript, the propulsive force for an ant may be written as the product of an activity coefficient k_a and $\boldsymbol{\eta}$, the two-dimensional standard normal distribution with zero mean and unit standard deviation. Effectively, $k_a\boldsymbol{\eta}$ is the Gaussian distribution with standard deviation k_a. At each time step, and for each ant i, we randomly sampled a value from this distribution. To measure activity level k_a, we first describe their trajectories.

Figure 2(A) shows an overlay of ten individual fire ant trajectories on the water surface. These trajectories are characterized by looping circular paths with straight-line distances of less than a few body lengths. Trajectories on water vary significantly from trajectories atop ant rafts, where their straight line distance is on the order of 4 cm, or over 13 body lengths [31]. For simplicity, ants in our model are considered circular discs with no heading.

The velocity distribution of ants on the water surface is qualitatively similar to that of Brownian particles such as pollen. **Figure 2**(B) shows the probability distribution of an ant's speed $U = \sqrt{u^2+v^2}$, where u and v are the x and y components of the ant's walking velocity $\dot{\boldsymbol{x}}_i = [u, v]$. The two insets of **Figure 2**(B) show that an ant's translational velocity components (u, v) are normally distributed around zero, indicating that ants have no directional bias. The standard deviation σ of velocity in either direction (u, v) is approximately 3.5 mm/s ($n = 96$). Ants on the water locomote at speeds of $U = 4.2 \pm 2.8$ mm/s ($n = 96$), a fifth of their walking speed on land, 20 mm/s [35]. Previous work reports that fire ants "showed no directed motion" and categorized them as non-swimmers compared to other tropical ant species [36]. Notably, fire ants are also smaller than other tropical species, which may make their locomotion less effective on water.

Following the prediction from statistical mechanics, **Figure 2**B shows the probability distribution of the velocity magnitude U, which is well approximated by the two-dimensional Maxwell-Boltzmann distribution (solid red line),

$$\mathrm{pdf}(U) = \frac{1}{2\pi\sigma^2} e^{-\frac{1}{2}(U/\sigma)^2} \tag{3}$$

where pdf is the probability distribution function, and σ is the standard deviation for u and v. The mean squared displacement (MSD) of ant trajectories is defined as

$$\mathrm{MSD}(\Delta t) = \left\langle |\boldsymbol{x}(t+\Delta t) - \boldsymbol{x}(t)|^2 \right\rangle, \tag{4}$$

where $\langle \ldots \rangle$ denotes the average over all samples and time t. **Figure 2**C shows the MSD of ant trajectories ($n = 96$), where MSD is in mm^2 and the time interval Δt is in seconds. The MSD reveals that the motion is ballistic at short times ($\sim 7.5\Delta t^2$ for $\Delta t < 5$ s, $R^2 = 0.97$) and diffusive at long times ($\sim 30\Delta t$ for $\Delta t > 8$ s, $R^2 = 0.98$). These statistical features confirm that the locomotion of fire ants on the water surface can be modeled by inertial random walkers such as dust particles in plasmas, mini-robots, and Whirligig beetles [37, 38].

The transition between the two regimes is smooth and we could not identify a critical threshold based on the MSD statistics alone. However, though the coasting dead ant experiments that we will introduce below, we calculate a time scale for inertial effects (vertical gray dashed line) that lies in the transition region of MSD.

Fitting the MSD at the early ballistic stage yields the characteristic velocity of 2.7 mm/s ($R^2 = 0.97$), comparable to the average speed in the histograms in **Figure 2**B. From the later diffusive phase, we calculate the diffusion coefficient D of 7.5 mm^2/s ($R^2 = 0.98$). This diffusion coefficient suggests that over 22 minutes, an ant's final position on water will be ten centimeters away from its initial position. We can relate the activity coefficient k_a in our model (Equation (2)) to the friction coefficient k_f through $k_a = k_f\sqrt{2D/\delta t}$ [37], where δt is the time step used in our simulations (see the Materials and Methods section).

Although we neglect turning in our model, we briefly explain the looping trajectories observed. Directional bias is absent in our experiments: the mean orientational velocity of the ants, $\dot{\theta}$, is negligible at -0.002 rad/s (n=97). Persistent turning explains the circular trajectories in **Figure 2**A. Fig. S1 shows that orientational MSD has a slope of 1.7 ($R^2 = 0.995$), indicating that ants' angular velocities are hyper-diffusive.

Fluid drag

The second term in Equation (2) is the fluid drag on an ant. We performed experiments by manually pushing dead ants by hand and recording their deceleration on the water surface due to hydrodynamic drag (Fig. S2). In the intermediate Re regime (Re$\sim$ 10), drag involves both pressure drag ($\sim U^2$) and viscous drag (proportional to $\sim U$). However, we found that viscous drag is sufficient to explain the deceleration. We fit the relationship between fluid drag and the velocity to obtain the coefficient $k_f = 0.24$ mg/s ($n = 14$, $R^2 = 0.82$). The time scale of the inertial effect $\tau = m/k_f = 4.3$ s approximately coincides with the transition between the inertial and diffusive regimes in MSD (vertical gray dashed line in **Figure 2**), as predicted by the Langevin model for Brownian particles. Indeed, in the absence of interaction terms, Equation (2) describes Brownian motion [37].

Capillary attraction

The last two terms of Equation (2) involve the interaction among individuals and vary with $\boldsymbol{d_{ij}} = \boldsymbol{x_i} - \boldsymbol{x_j}$, the distance between a pair of ants. Small floating objects such as paperclips or Cheerios are drawn together by capillary forces, which act to minimize the deformation of the water surface. Similarly, in both experiments with live and dead ants, we observe attraction sufficient to draw ants together if the initial distance is within a few centimeters. Nicolson et al. derived the attraction force between two floating spheres

$$F_c = k_c \mathrm{K}_1(d/l_c), \tag{5}$$

where k_c is a fitting parameter measured from experiments, K_1 is the modified Bessel function, d is the distance between the two objects, and $l_c = 2.7$ mm is the capillary length of water. The

parameter k_c depends on the geometry, contact angle, and density of the object [39, 40, 41]. We account for these effects by fitting the interaction between two dead ants. Although ants are elongated and have a rough surface, we neglect these second-order effects and focus on representing the capillary attraction between ants as floating spheres. Through measuring the attraction between pairs of dead ants (see the method section and Fig. S3), we obtain $k_c = 2.6$ nN ($n = 33$, $R^2 = 0.83$). Based on the value of k_c, the attraction force between two ants is comparable to the attraction between a pair of small plastic spheres (diameter 1 mm, density 1.1 g/mL, and contact angle 70°).

Short-range repulsion

The last term in Equation (2) is the short-range elastic repulsion force when two ants collide. In simulations, we approximate ants as a 2D discs with radius $r = 1$ mm, which was chosen to be both comparable to the ant length l and ant width w. Collisions occur when the inter-ant distance $d_{ij} < 2r$. Our simulation results were comparable for most non-zero values of k_r; therefore we used $k_r = 0.05$ nN/mm.

Our final model, Equation (2), is capable of simulating the trajectories of arbitrary numbers of ants. Except for k_r, which was set to avoid overlapping agents when they came too close, there were no free parameters in our model; all parameters were measured from our experiments on both live and dead ants. In the Materials and Methods section, we detail how we measure the four model parameters (k_a, k_f, k_c, k_r) that characterize the four forces acting on the ants.

Multi-agent simulations capture the stability transition

In this section, we present simulations of raft destabilization and raft formation, in which we vary factors that would be difficult to change experimentally.

Raft destabilization simulations begin with ants in a hexagonal lattice, the tightest possible configuration for monodisperse discs. We perform 150 simulations with 15 different raft sizes and 10 numerical trials with different values for the random variable $\boldsymbol{\eta}$ which describes their diffusion. **Figure 3**A and Movie S2 demonstrate that assemblies of seven agents disintegrate, while rafts of 19 agents remain stable, similar to the behavior observed in experiments. **Figure 1**B shows P, the proportion of stray ants at the end of the trial of five minutes, decreases with the number of ants N in simulations (gray circles). We fit the simulation results to the logistic function, Equation (1), finding that the critical number of ants $N_c = 9.5$ and $\Delta N = 1.1$ ($n = 150, R^2 = 0.88$), matching the experimental logistic function well. We thus conclude that the stability transition emerges from the agent interactions in our model, the combination of random walks, drag, contact repulsion, and Cheerios effects (**Figure 3**B). We next use our model to explore the effect of activity levels and the initial spacing of ants.

Next, we consider the effect of ant activity on raft stability. In our experiments, we observed that the leg motion of fire ants dwindles over time. Immediately after being placed on water, ants flail their legs at 20.2 ± 4.5 mm/s ($n = 6$) at their tips. The movement slows down to 10.0 ± 4.5 mm/s ($n = 6$) over a span of ten minutes. This slow down with time is consistent with our previous findings that ants reduce exploration and metabolism with time [42, 33]. Could the decrease in activity improve the stability of the rafts? To answer this question, we simulated ants with activity coefficient k_a ranging from 0.5 to 3.4 nN, where the activity level measured from our experiments was 3.0 nN. **Figure 3**C shows the stability diagram of the rafts ($n = 1200$). Larger rafts with less active ants are more stable, as expected. This black dashed curve represents the critical size where half of the ants remain stable in the raft ($P = 0.5$); by fitting to an exponential, we find this stability criteria correspond to $N_c \approx 0.3e^{1.2k_a}$.

Now that we have identified how ant rafts remain stable, we investigate how rafts are assembled in the first place. These simulations were conducted with ants in a square lattice of centroid-to-centroid spacing L. **Figure 4**a shows the proportion of ants that remain isolated after five minutes as a function of the activity level and initial spacing L. Each data point is an average of ten numerical trials per condition ($n = 660$). For ants to assemble into a raft from a dispersed state, they must be sufficiently close together. Closely spaced ants with a spacing of $L = 16.7$ mm condense into rafts if the activity is sufficiently low. Higher activity levels lead to collisions that destabilize the aggregation. Conversely, distant ants with spacing $L = 37.5$ mm rarely encounter any neighbors within five minutes if their activity is low ($k_a = 0.5$ nN). This phenomenon is observed in our experiments: satellite ants a few centimeters away from their neighbors remain isolated if their activity level is too low. Ants must actively locomote on the water surface to encounter neighboring ants. In our experiments, as ant activity levels naturally dwindle with time, sparsely distributed ants have increasing difficulty encountering neighbors. Therefore, the initial spacing is a critical factor for raft formation.

Figure 4B-C demonstrate the time series of stray ant proportions P for various activity levels and two initial ant-to-ant spacing, L, of 18.75 mm and 30 mm. At small ant-to-ant spacing, $L = 18.75$ mm, even though the proportion of ants P at $t = 5$ min is monotonic with activity, the time-scale to achieve 50 percent assembly is nonlinear. Such nonlinearity is due to the pros and cons of increasing activity levels: namely, high activity enables ants to find one another but impedes raft formation upon contact. Conversely, ants of low activity level take longer to find one another but stick together better once in contact. When the activity is low at $k_a = 0.5$ nN, rafts assemble slower because it takes longer for ants to find their neighbors. For large ant-to-ant spacing $L = 30$ mm, even though low-activity ants assemble more slowly, newly formed rafts rarely break apart. The comparison between **Figure 4**B and **Figure 4**C reveal that for any fixed activity level k_a, the raft is established more rapidly at low initial spacings (**Figure 4**C). At the spacing of $L = 18.75$ mm, except for when $k_a = 1.5$ nN, the system either quickly converges to the aggregated state ($k_a < 1.5$ nN), or maintains the dispersed state ($k_a > 1.5$ nN).

Discussion

Phase-transition analogy of raft stability

Animal swarms can display both behavioral phases (such as Pharaoh ant trail-following [43], and desert locust swarming [44, 45]) and thermodynamical phases [46, 47, 48, 49, 50, 51, 52]. The assembly and disassembly of fire ant rafts is analogous to the phase transition of non-living materials such as water. Here, the raft may be considered the liquid phase; and the dispersed ants, the vapor phase. Subsequently, the proportion of stray ants is analogous to the vapor quality. In this viewpoint, we can readily compare **Figure 4**A to the T-V diagram of the water, where the temperature T corresponds to the ant activity and volume V corresponds to the number of ants.

Following the statistical mechanics' framework and assuming detailed balance, we may also estimate the effective temperature $T_{activity} = 1.4 \times 10^{13}$ K using the Stokes-Einstein relation $D = \frac{k_B T_{activity}}{6\pi\mu l}$, where k_B is the Boltzmann constant, μ the viscosity of water and l the length of the ants. We can estimate the pressure per unit depth $P_{activity}$ by equating the energy scales (ideal gas law) $P_{activity}A = k_B T_{activity}$, where A is the surface area of an ant. We obtain $P_{activity} = 0.2$ mN/m, which is around 1/300 of the water surface tension. Note that the pressure drives ants apart, and surface tension pulls them together.

Fire ant rafts constantly expend energy and are thus out of equilibrium, departing from most traditional physical systems. From previous work, we know that ants slow down and ant rafts shrink

on the order of hours [33]. To avoid these fatigue effects, which are difficult to model, we chose five minutes as the time frame to perform our observations and simulations. The numbers calculated will vary with the time frame chosen, but the physical picture should remain the same. Further understanding of the collective dynamics of biological systems calls for a statistical mechanical framework that permits temporal variability as well as individual differences.

Biological assemblies on the water surface

Can our model predict if and under what conditions other species can aggregate? Three factors should be considered. Different animals have different physical properties (density, size, hydrophobicity, etc.), and thus different coefficients for the Cheerios effect attraction k_c. While ants are well described by random walks, other organisms may need different models. For example, the locomotion of whirligig beetles resembles "corralled active Brownian particles" [53]. Chirality is critical in describing starfish embryo assemblies [54].

Recently, biologists have identified more ant species that can build rafts, including *Pheidole*, *Formica*, *Wasmannia*, and *Linepthema* spp. [36, 55, 56, 57, 58, 59]. They are often found in habitats prone to inundation. Notably, one common feature of these rafting species is their small body size (< 1 cm), hinting at the potential significance of surface tension and the Cheerios effect in their assembly mechanism. Comparative studies of these species that test the predictive power of our model would be an exciting future direction.

As we focus on the fire ant behaviors on the water surface over a short time scale (five minutes), it can be argued that ants have very limited sensory capabilities. Indeed, we demonstrate that ants walking on the water surface cannot recognize neighboring ants and ricochet off them. The nature of the system calls for stochastic dynamics, where the activity is modeled as white noise that does not require any memory or feedback loop. The lack of memory or feedback is similar for swarms of black soldier larvae as well [60].

Our research coincides with active matter beyond the over-damped limit [61, 38, 62, 53]. Löwen has shown that rich physics can arise from the addition of the inertial term, such as the co-existence of different temperature phases [38]. There has also been increasing interest in active matter at the fluid interfaces [63, 64, 65, 53, 54, 66]. Our model, Equation (2), shares significant similarity with these systems. Through this combined experimental and theoretical study, we present fire ants as a model system for future explorations on these topics.

Conclusion

We have shown that fire ants cohere on the water surface through capillary forces. Remarkably, the activity of the ants destabilizes the assembly, causing small rafts to disintegrate. We used a Langevin model to simulate raft breakages and reproduced the stability transition condition we discovered in experiments. Further, we used the model to predict the initial ant spacing required to assemble rafts.

Materials and methods

Raft experiments

Fire ant colonies were collected from the campus of Georgia Institute of Technology, Atlanta, Georgia. We kept them in plastic trays with access to water and food. In all collected colonies,

multiple queens were found. To reduce the effects of the artificial rearing environment in the lab, we only used ants harvested within three months for experiments.

To make rafts, we used previously published protocols [31]: we selected ants from a colony and placed them into a beaker coated with Insect-a-Slip. Then we swirled the beaker to roll the ants into a ball and placed the ball on the water surface. Ants fewer than 30 in number were manually counted before the experiment. For larger numbers, the beaker was weighed and converted to the number of ants using the average weight of one ant, which was around one milligram. For five minutes, we recorded the trajectories of ants and counted the number of stray ants at the end of the film.

Measuring parameters for the Langevin model

We tracked 96 ants to determine their activity level on the water surface. Ants were picked up from the colony using tweezers and transferred to the water surface by gently tapping the tweezers. Occasionally, ants landed on their back and could not flip over due to surface tension. These trials were excluded from further analysis. We recorded the trajectories of ants using an Opti-Tekscope USB microscope placed above the water surface. The recordings were analyzed using a custom MATLAB tracking program. The same system was used to obtain the trajectories in the following experiments.

To measure drag coefficient k_f and the Cheerios effect coefficient k_c, we used recently deceased ants. We euthanized the ants by placing them in the freezer for around ten minutes. We used tweezers to straighten the ants' bodies and legs before placing them on the water surface. We gently pushed the ant so that it started drifting with an initial velocity. We recorded 14 trajectories as they decelerated due to fluid drag. We used Gaussian smoothing and forward difference to calculate the velocity using a time interval of 0.06 s. We find that velocity decreases exponentially with time (Fig S2), suggesting that fluid drag is proportional to the velocity magnitude. We obtain the coefficient for drag k_f from fitting a straight line to the relationship between the logarithm of velocity $\log(U)$ and time t. We measured k_f to be 0.24 mg/s ($n = 14$, $R^2 = 0.82$, Fig. S2).

The activity coefficient k_a depends on both drag coefficient k_f and the time step δt. For intuition, consider the random propulsion term $k_a \boldsymbol{\eta}$ as an average value over a period of δt. The larger the δt, the more smoothed out the random signal becomes in each period, hence the smaller the activity coefficient k_a. To estimate k_a, we used $\delta t = 0.1$ s, the same value that we used for integrating Equation (2) in the simulations. Together, we obtained $k_a = k_f\sqrt{2D/\delta t} = 2.88$ nN. Detailed derivation of this relationship may be found in the supplemental materials.

The Cheerios effect coefficient k_c was measured by placing two dead ants on the water surface. Through the same procedure above, we calculated the relative velocity and acceleration as they attracted each other. The attractive force was calculated as the sum of inertia and fluid drag terms of the Langevin model, Equation (2). Fig. S3 shows that the attraction force decreases monotonically with the distance between the ants. We fit the data to the modified Bessel functions, which we expect from theory [41, 40, 39]. We arrived at $k_c = 2.56$ nN ($n = 33$, $R^2 = 0.83$).

Simulation

We performed 1860 agent-based simulations in MATLAB, consisting of 1200 simulations for raft destabilization and 660 for raft assembly. Raft destabilization simulations were performed with ants initially on a hexagonal lattice, and raft assembly simulations with a square lattice. Circular agents were characterized using four coefficients measured from experiments (m, k_a, k_f, k_c) and one free parameter, the close-range repulsion k_r that had little effect on the results when it was above

the chosen value. At each time step, the location and the velocity of each agent were updated according to Equation (2). For raft destabilization simulations, we integrated the equations with a semi-explicit scheme with a time step of $\delta t = 0.1$ s. For each parameter combination, we simulated five minutes of ant motion. The results were averaged over ten trials with different seeds for random number generators.

For raft assembly simulations, we started the simulations from agents on square lattices. The simulation domain was a square that was 150 body radii wide. Periodic boundary condition was imposed in both directions so that the density within the domain remained constant. At the beginning of the simulations, agents were placed in 4x4 to 9x9 square formations. Similar to the raft destabilization trials, we simulated five minutes of ant motion, and results were obtained after averaging over ten realizations.

Acknowledgement

This work is funded by Army Research Office (W911NF-19-1-0086) and Presidential Undergraduate Research Award (PURA) at Georgia Institute of Technology. We greatly appreciate Prof. Zeb D. Rocklin for helpful discussions on statistical mechanics and reviewers for their feedback.

References

[1] Anderson, C., Theraulaz, G. & Deneubourg, J.-L. Self-assemblages in insect societies. *Insectes sociaux* **49**, 99–110 (2002).

[2] Sumpter, D. J. The principles of collective animal behaviour. *Philosophical transactions of the royal society B: Biological Sciences* **361**, 5–22 (2006).

[3] Camazine, S. *et al. Self-organization in biological systems* (Princeton university press, 2020).

[4] Reid, C. R. *et al.* Army ants dynamically adjust living bridges in response to a cost–benefit trade-off. *Proceedings of the National Academy of Sciences* **112**, 15113–15118 (2015).

[5] Bonner, J. T. A descriptive study of the development of the slime mold dictyostelium discoideum. *American Journal of Botany* 175–182 (1944).

[6] Bonner, J. T. & Frascella, E. B. Variations in cell size during the development of the slime mold, dictyostelium discoideum. *The Biological Bulletin* **104**, 297–300 (1953).

[7] Weihs, D. Hydromechanics of fish schooling. *Nature* **241**, 290–291 (1973).

[8] Liao, J. C., Beal, D. N., Lauder, G. V. & Triantafyllou, M. S. Fish exploiting vortices decrease muscle activity. *Science* **302**, 1566–1569 (2003).

[9] Liao, J. C. A review of fish swimming mechanics and behaviour in altered flows. *Philosophical Transactions of the Royal Society B: Biological Sciences* **362**, 1973–1993 (2007).

[10] Ward, A. & Webster, M. *Sociality: The Behaviour of Group-Living Animals* (Springer International Publishing, 2016). URL `http://link.springer.com/10.1007/978-3-319-28585-6`.

[11] Grégoire, G. & Chaté, H. Onset of collective and cohesive motion. *Physical review letters* **92**, 025702 (2004).

[12] Aoki, I. A simulation study on the schooling mechanism in fish. *Bulletin of the Japanese Society of Scientific Fisheries* **48**, 1081–1088 (1982).

[13] Reynolds, C. W. Flocks, herds and schools: A distributed behavioral model. In *Proceedings of the 14th annual conference on Computer graphics and interactive techniques*, 25–34 (1987).

[14] Huth, A. & Wissel, C. The simulation of the movement of fish schools. *Journal of theoretical biology* **156**, 365–385 (1992).

[15] Couzin, I. D., Krause, J., James, R., Ruxton, G. D. & Franks, N. R. Collective memory and spatial sorting in animal groups. *Journal of theoretical biology* **218**, 1–11 (2002).

[16] Shimoyama, N., Sugawara, K., Mizuguchi, T., Hayakawa, Y. & Sano, M. Collective motion in a system of motile elements. *Physical Review Letters* **76**, 3870 (1996).

[17] Vicsek, T., Czirók, A., Ben-Jacob, E., Cohen, I. & Shochet, O. Novel type of phase transition in a system of self-driven particles. *Physical review letters* **75**, 1226 (1995).

[18] Grégoire, G., Chaté, H. & Tu, Y. Moving and staying together without a leader. *Physica D: Nonlinear Phenomena* **181**, 157–170 (2003).

[19] Couzin, I. D., Krause, J. *et al.* Self-organization and collective behavior in vertebrates. *Advances in the Study of Behavior* **32**, 10–1016 (2003).

[20] Katz, Y., Tunstrøm, K., Ioannou, C. C., Huepe, C. & Couzin, I. D. Inferring the structure and dynamics of interactions in schooling fish. *Proceedings of the National Academy of Sciences* **108**, 18720–18725 (2011).

[21] Herbert-Read, J. E. *et al.* Inferring the rules of interaction of shoaling fish. *Proceedings of the National Academy of Sciences* **108**, 18726–18731 (2011). URL `https://www.pnas.org/content/108/46/18726`. `https://www.pnas.org/content/108/46/18726.full.pdf`.

[22] Hinz, R. C. & de Polavieja, G. G. Ontogeny of collective behavior reveals a simple attraction rule. *Proceedings of the National Academy of Sciences* **114**, 2295–2300 (2017).

[23] Zienkiewicz, A. K., Ladu, F., Barton, D. A., Porfiri, M. & Di Bernardo, M. Data-driven modelling of social forces and collective behaviour in zebrafish. *Journal of Theoretical Biology* **443**, 39–51 (2018).

[24] Ballerini, M. *et al.* Interaction ruling animal collective behavior depends on topological rather than metric distance: Evidence from a field study. *Proceedings of the national academy of sciences* **105**, 1232–1237 (2008).

[25] Bialek, W. *et al.* Statistical mechanics for natural flocks of birds. *Proceedings of the National Academy of Sciences* **109**, 4786–4791 (2012).

[26] Lukeman, R., Li, Y.-X. & Edelstein-Keshet, L. Inferring individual rules from collective behavior. *Proceedings of the National Academy of Sciences* **107**, 12576–12580 (2010).

[27] Puckett, J. G., Kelley, D. H. & Ouellette, N. T. Searching for effective forces in laboratory insect swarms. *Scientific reports* **4**, 1–5 (2014).

[28] Lopez, U., Gautrais, J., Couzin, I. D. & Theraulaz, G. From behavioural analyses to models of collective motion in fish schools. *Interface focus* **2**, 693–707 (2012).

[29] Tschinkel, W. R. *The fire ants* (Belknap Press, 2013).

[30] Morrison, L. W., Porter, S. D., Daniels, E. & Korzukhin, M. D. Potential global range expansion of the invasive fire ant, solenopsis invicta. *Biological invasions* **6**, 183–191 (2004).

[31] Mlot, N. J., Tovey, C. A. & Hu, D. L. Fire ants self-assemble into waterproof rafts to survive floods. *Proceedings of the National Academy of Sciences* **108**, 7669–7673 (2011).

[32] Wagner, R. J., Such, K., Hobbs, E. & Vernerey, F. J. Treadmilling and dynamic protrusions in fire ant rafts. *Journal of the Royal Society Interface* **18**, 20210213 (2021).

[33] Ko, H., Yu, T.-Y. & Hu, D. L. Fire ant rafts elongate under fluid flows. *Bioinspiration & Biomimetics* **17**, 045007 (2022). URL `https://doi.org/10.1088/1748-3190/ac6d98`.

[34] Mlot, N. J., Tovey, C. & Hu, D. L. Dynamics and shape of large fire ant rafts. *Communicative & integrative biology* **5**, 590–597 (2012).

[35] Morrill, W. L. Red imported fire ant foraging in a greenhouse. *Environmental entomology* **6**, 416–418 (1977).

[36] Yanoviak, S. P. & Frederick, D. Water surface locomotion in tropical canopy ants. *Journal of Experimental Biology* **217**, 2163–2170 (2014).

[37] Pathria, R. K. & Beale, P. D. *Statistical Mechanics* (Elsevier/Academic Press, 2011), 3rd ed edn.

[38] Löwen, H. Inertial effects of self-propelled particles: From active brownian to active langevin motion. *The Journal of chemical physics* **152**, 040901 (2020).

[39] Nicolson, M. M. The interaction between floating particles. *Mathematical Proceedings of the Cambridge Philosophical Society* **45**, 288â€“295 (1949).

[40] Chan, D., Henry Jr, J. & White, L. The interaction of colloidal particles collected at fluid interfaces. *Journal of Colloid and Interface Science* **79**, 410–418 (1981).

[41] Vella, D. & Mahadevan, L. The "cheerios effect". *American journal of physics* **73**, 817–825 (2005).

[42] Ko, H., Komilian, K., Waters, J. S. & Hu, D. L. Metabolic scaling of fire ants (Solenopsis invicta) engaged in collective behaviors. *Biology Open* **11** (2022). URL `https://doi.org/10.1242/bio.059076`. Bio059076, `https://journals.biologists.com/bio/article-pdf/11/2/bio059076/2141612/bio059076.pdf`.

[43] Beekman, M., Sumpter, D. J. & Ratnieks, F. L. Phase transition between disordered and ordered foraging in pharaoh's ants. *Proceedings of the National Academy of Sciences* **98**, 9703–9706 (2001).

[44] Simpson, S. J., McCaffery, A. R. & Hägele, B. F. A behavioural analysis of phase change in the desert locust. *Biological reviews* **74**, 461–480 (1999).

[45] Ariel, G. & Ayali, A. Locust collective motion and its modeling. *PLOS Computational Biology* **11**, e1004522 (2015).

[46] Ling, H. *et al.* Behavioural plasticity and the transition to order in jackdaw flocks. *Nature communications* **10**, 1–7 (2019).

[47] Nave Jr, G. K. *et al.* Attraction, dynamics, and phase transitions in fire ant tower-building. *Frontiers in Robotics and AI* **7**, 25 (2020).

[48] Chen, Y. & Ferrell, J. E. C. elegans colony formation as a condensation phenomenon. *Nature communications* **12**, 1–10 (2021).

[49] Liu, Q.-X. *et al.* Phase separation explains a new class of self-organized spatial patterns in ecological systems. *Proceedings of the National Academy of Sciences* **110**, 11905–11910 (2013).

[50] Becco, C., Vandewalle, N., Delcourt, J. & Poncin, P. Experimental evidences of a structural and dynamical transition in fish school. *Physica A: Statistical Mechanics and its Applications* **367**, 487–493 (2006).

[51] Liu, G. *et al.* Self-driven phase transitions drive myxococcus xanthus fruiting body formation. *Physical review letters* **122**, 248102 (2019).

[52] Sinhuber, M. & Ouellette, N. T. Phase coexistence in insect swarms. *Physical review letters* **119**, 178003 (2017).

[53] Devereux, H. L., Twomey, C. R., Turner, M. S. & Thutupalli, S. Whirligig beetles as corralled active brownian particles. *Journal of the Royal Society Interface* **18**, 20210114 (2021).

[54] Tan, T. H. *et al.* Development drives dynamics of living chiral crystals (2021). `2105.07507`.

[55] Nielsen, M. G. Ants (hymenoptera: Formicidae) of mangrove and other regularly inundated habitats: life in physiological extreme. *Myrmecological News* **14**, 113–121 (2011).

[56] Lude, A., Reich, M. & Plachter, H. Life strategies of ants in unpredictable floodplain habitats of alpine rivers (hymenoptera: Formicidae). *Entomologia Generalis* 75–91 (1999).

[57] Purcell, J., Avril, A., Jaffuel, G., Bates, S. & Chapuisat, M. Ant brood function as life preservers during floods. *PloS one* **9**, e89211 (2014).

[58] Avril, A., Purcell, J. & Chapuisat, M. Ant workers exhibit specialization and memory during raft formation. *The Science of Nature* **103**, 1–6 (2016).

[59] Fernandes, G. W., de Castro, F. S., Camarota, F., Blum, J. C. & Maia, R. Ant rafting in an extreme ecosystem. *Sociobiology* **68**, e7430–e7430 (2021).

[60] Ko, H. *et al.* Air-fluidized aggregates of black soldier fly larvae. *Frontiers in Physics* **9** (2021). URL `https://www.frontiersin.org/articles/10.3389/fphy.2021.734447`.

[61] Klotsa, D. As above, so below, and also in between: mesoscale active matter in fluids. *Soft matter* **15**, 8946–8950 (2019).

[62] Zampetaki, A. V., Liebchen, B., Ivlev, A. V. & Löwen, H. Collective self-optimization of communicating active particles. *Proceedings of the National Academy of Sciences* **118** (2021).

[63] Deng, J., Molaei, M., Chisholm, N. G. & Stebe, K. J. Motile bacteria at oil–water interfaces: Pseudomonas aeruginosa. *Langmuir* **36**, 6888–6902 (2020).

[64] Molaei, M., Chisholm, N. G., Deng, J., Crocker, J. C. & Stebe, K. J. Interfacial flow around brownian colloids. *Physical Review Letters* **126**, 228003 (2021).

[65] Thomson, S. & Harris, D. Non-equilibrium capillary self-assembly. *Bulletin of the American Physical Society* **66** (2021).

[66] Chisholm, N. G. & Stebe, K. J. Driven and active colloids at fluid interfaces. *Journal of Fluid Mechanics* **914** (2021).

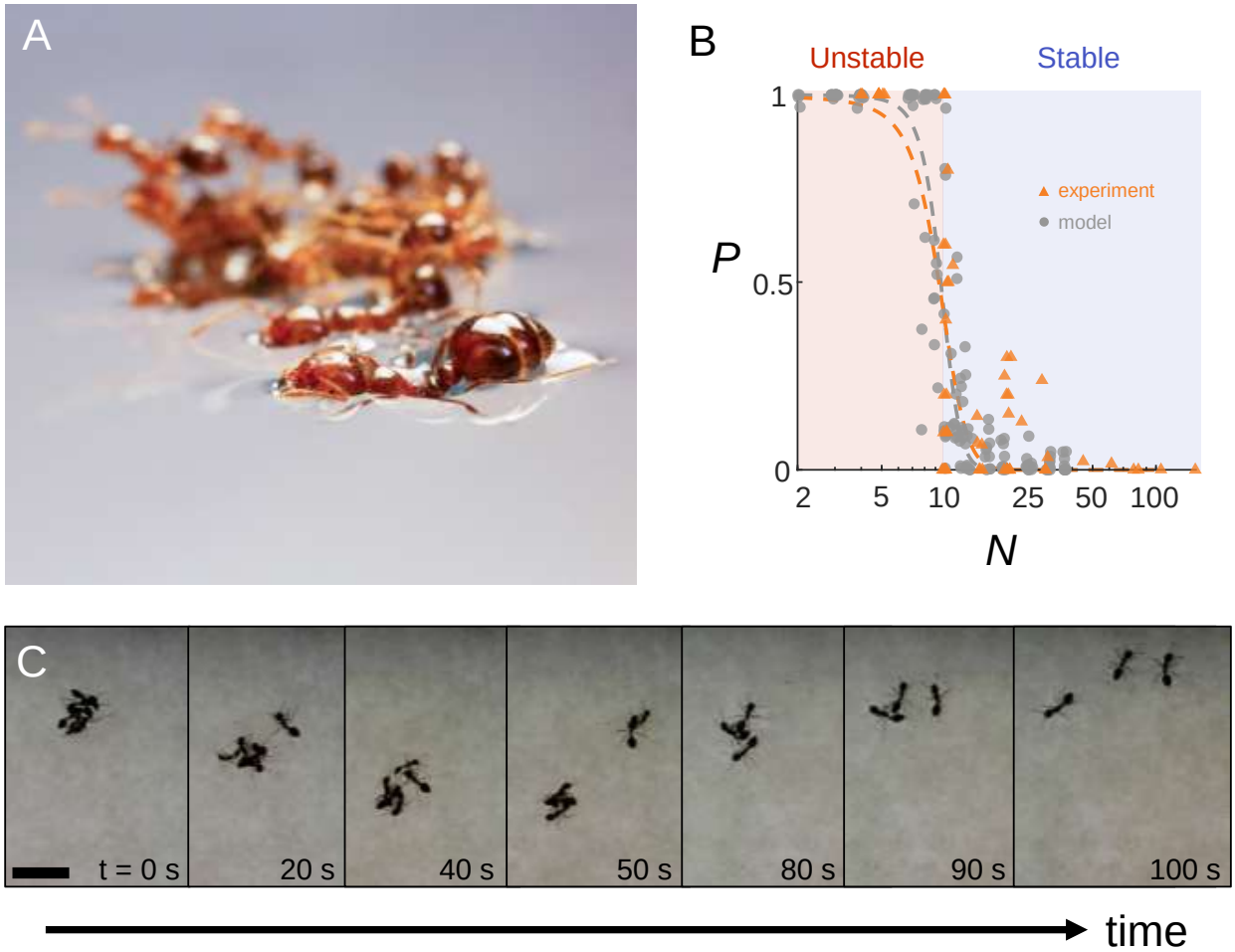

Figure 1: Small rafts are unstable. (A) A raft of twenty ants on the surface of water. (Photo credits: Andre L Magyar and Candler Hobbs) (B) Proportion of stray ants P as a function of the raft size N. Orange triangles indicate experimental results ($n = 72$) and gray circles simulation results ($n = 150$). Orange and gray dashed lines represent the respective best-fit logistic functions for experiments and simulation. (C) A time series showing the destabilization of raft of five ants over 100 s. Scale bar is 1 cm.

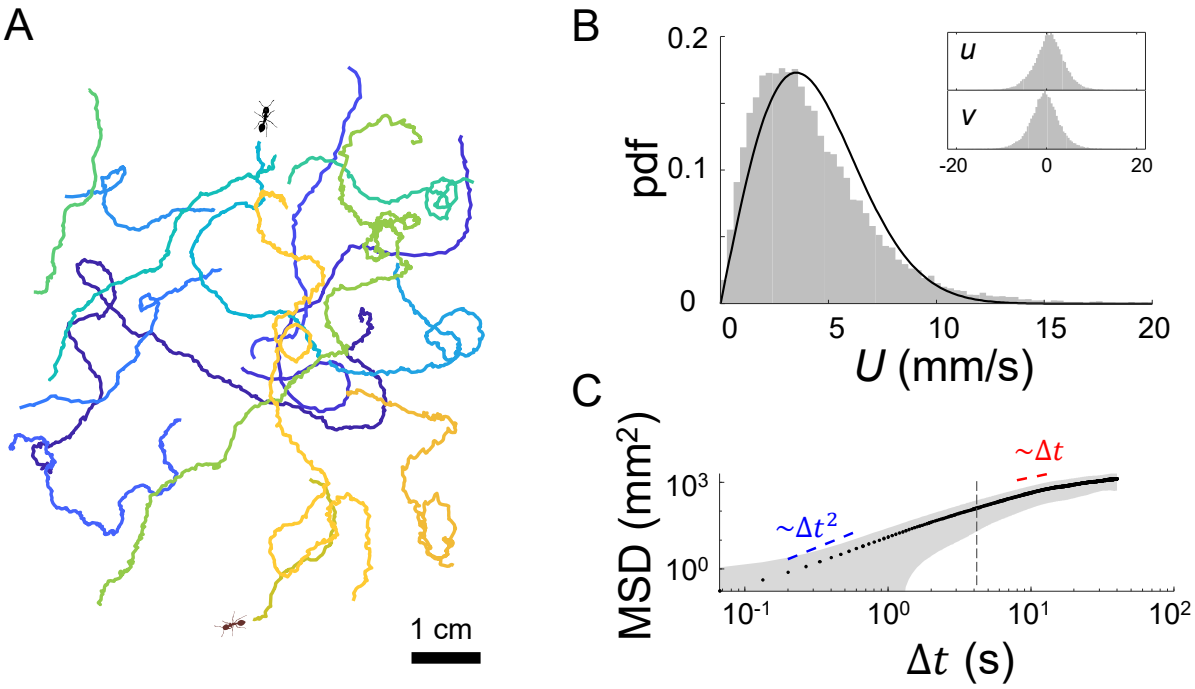

Figure 2: Ants on the water surface behave as inertial random walkers. (A) Ten representative ant trajectories. (B) Probability distribution of the velocity magnitude U. Velocity components u and v are shown in the insets. The red solid line is the two-dimensional Maxwell-Boltzmann distribution with a standard deviation 3.5 mm/s. (C) Mean squared displacement of ant trajectories. The blue dashed line has a slope of 2 and the red a slope of 1, and both are offset from the best fit for clarity. The vertical gray dashed line marks the time scale we obtain through a separate series of experiments $\tau = m/k_f$ 4.3 s. The shaded area represents one standard deviation, which appears distorted under the logarithmic scale. $n = 96$ for both (B) and (C)

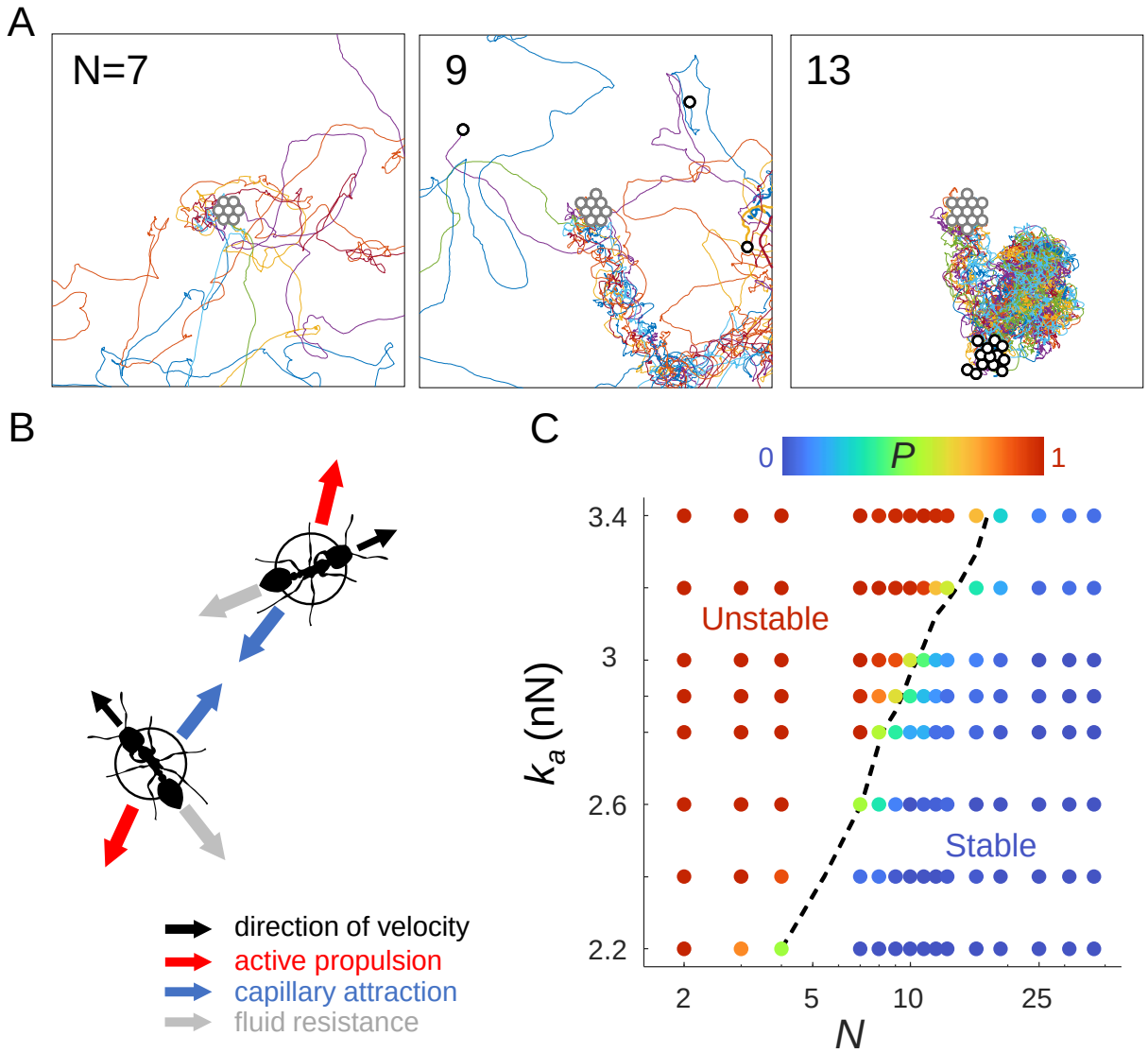

Figure 3: Destabilization of simulated ant rafts. (A) Trajectories of simulated ants as they start from a dense, ordered raft. Initial state of ants shown in red circles and end state shown with black circles. Note that many of the ending states have gone beyond boundaries of the figure. As the number of ants on the raft increases from 7 ants (left) to 9 ants (middle), and to 13 ants (right), rafts become more stable. (B) Schematic of our Langevin model (Equation (2)). (C) Raft stability diagram. Color represents the proportion of stray ants P after five minutes. Black dashed line marks the transition point where half of the ants go astray ($P = 0.5$).

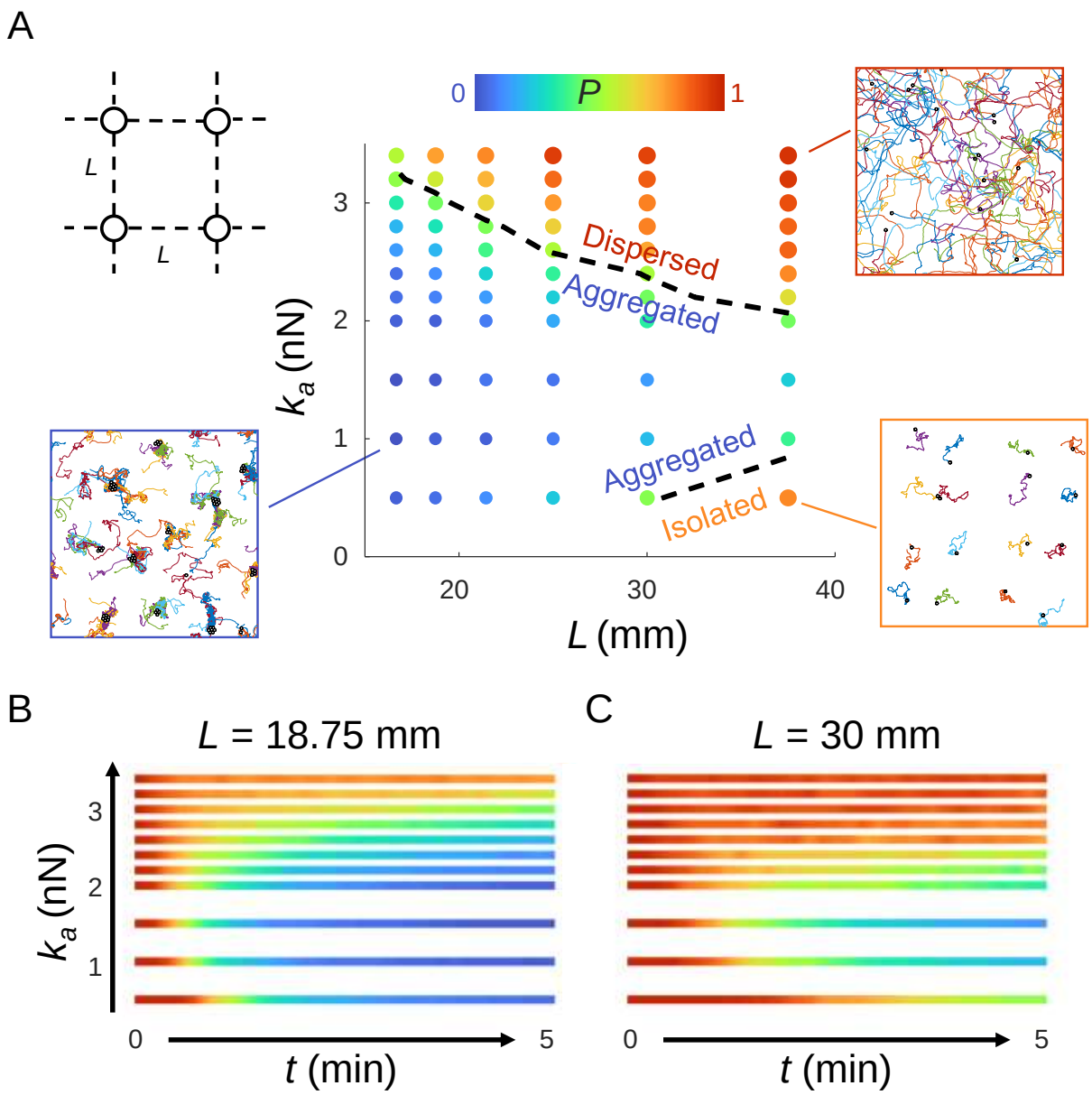

Figure 4: Assembly of ant rafts from different initial spacings. (A) Proportion of stray ants P as a function of activity level k_a and initial spacing L. Top left inset show the definition of initial ant spacing L. The remaining insets show representative trajectories of ants across a time frame of five minutes. Time series of P for (B) small initial spacing $L = 18.75$ mm and (C) large initial spacing 30 mm. Color represents the P for all subplots.